THE ARCHIVE OF MECHANICAL ENGINEERING

Vol. XLVIII 2001 Number 4

Key words: *composites, reinforced beams, fracture mechanic, photoelastic method, finite element method*

MIECZYSŁAW JARONIEK[*)]

EXPERIMENTAL AND NUMERICAL ANALYSIS OF THE REINFORCED COMPOSITE ELEMENTS SUBJECTED TO BENDING

Brittle fracture of the reinforced composite element has been a matter of considerable concern to engineers for many years. It is now generally accepted that the mode of failure is the centerpiece of the problem. The publication presents the experimental and numerical procedure used to determine the state of the stress in the photoelastic model of reinforced beams. The fracture process of fiber reinforced composite materials is very complicated, and the fracture strength is affected by: matrix cracking, fiber breakage and interfacial debonding between matrix and fibers.

The criterion used to calculate the maximum load was derived based on two processes only: matrix cracking and deformation of the reinforcement. The theoretical ultimate bending moment was calculated using the strain energy release rate G_C and the stress intensity factors (K_{II} and K_I) corresponding to the crack propagation of the matrix and the elastic-plastic deformation or the yield limit of the reinforcement.

1. Introduction

In calculating bending stresses in reinforced-composite beams, one commonly assumes that all the tension is taken by the fibbers and all the compression by the matrix.

It is the usual practice in calculating stresses in reinforced-composite beams to assume that Hooke's law holds for composite, and to compensate for the variable modulus by taking a lower value for this modulus than that obtained from compression tests. The optical properties of epoxy resin makes it possible to determine the stresses in the matrix by photoelastic method [2]. The dimensions of the typical model used in the experiment and material properties

[*)] *Technical University of Lodz, Faculty of Mechanical Engineering; ul. Stefanowskiego 1/15, 90-924 Łódź, Poland; E-mail: mjaro@ck-sg.p.lodz.pl*

are given in Fig. 1. The brittle fracture of the matrix was simulated by introduction of artificially initiated small cracks (notched) in the tension zone.

The stress distribution in the matrix was characterized by isochromatic patterns and the displacements were measured by applying strain gauges.

The fracture mechanics parameters: the stress intensity factors K_I, K_{II} and the strain energy release rate (G_C) were determined experimentally. The stress intensity factors: K_{IC} and K_{IIC} were evaluated from the load-displacement curve under the ASTM E813-81 standard and by using the photoelastic measurement results.

a)

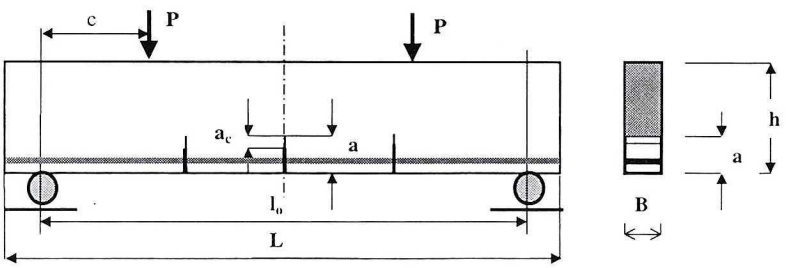

b)

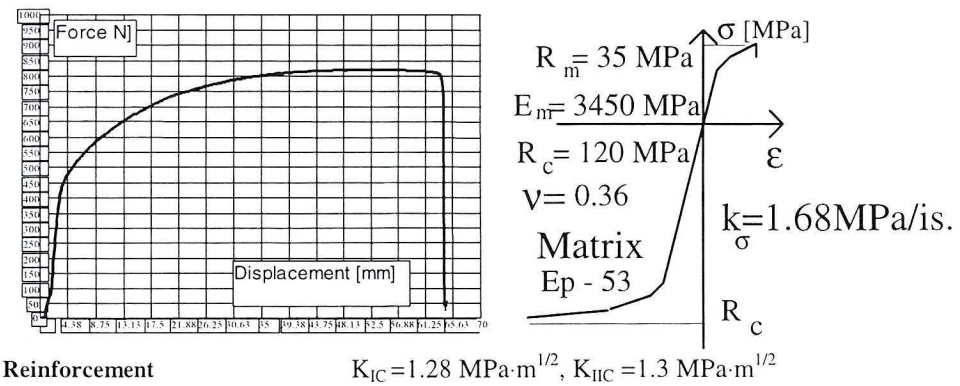

Reinforcement $K_{IC}=1.28$ MPa·m$^{1/2}$, $K_{IIC}=1.3$ MPa·m$^{1/2}$

c)

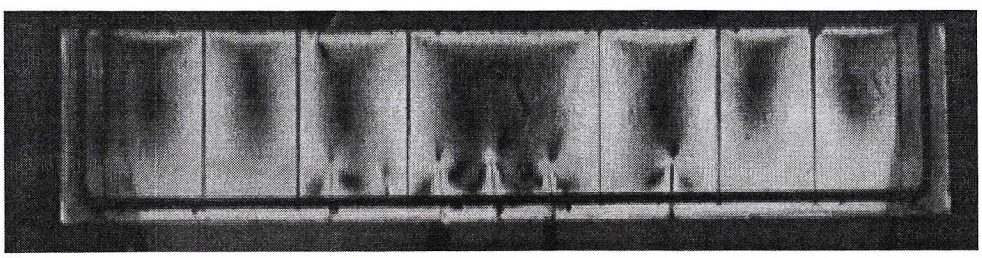

Fig.1. a) Typical details of the photoelastic models of the reinforced beams; b) Properties of the reinforcement and the matrix; c) Model reinforced linearly by carbon fibbers before test

2. Material properties

The properties of the matrix and the reinforcement were determined experimentally. The loading experiments were performed using displacement control method with automatic measurement system. The mechanical properties of the matrix were characterized by:

$\mathbf{E_m}$ = 3450 MPa	– Young's modulus,
ν_m = 0.36	– Poisson's ratio,
$\mathbf{R_c}$ =120 MPa, $\mathbf{R_m}$ =35 MPa	– ultimate strength (in: compression, tension),
$\mathbf{G_{IC}} \cong$ 0.5 kN/m	– critical value of the strain energy release rate,
$\mathbf{K_{IC}}$ =1.30 MPa·m$^{1/2}$, $\mathbf{K_{IIC}}$ =1.302 MPa·m$^{1/2}$	– critical values of the stress intensity factors,
$\mathbf{k_\sigma}$ =1.68 MPa/fr.	– photoelastic constants in terms of stresses,

and of the reinforcement:

$\mathbf{E_r}$ = 9.4·10^4 MPa	– Young's modulus,
ν_r = 0.29	– Poisson's ratio,
$\mathbf{R_e}$ =188 MPa, $\mathbf{R_m}$ = 320 MPa	– yield limit and ultimate strength in tension,

and load-displacement curve (σ-ε).

2.1. Fracture mechanics parameters

The stress intensity factors K_{IC} and K_{IIC} were evaluated from the load-displacement curve using the compact tension CT and compact shear CS specimens and the beams subjected to pure bending and asymmetric loading, as illustrated in Figs. 3 and 5. One applied the photoelastic measurement results verified using the method presented in [3]–[8]. The stress intensity factor K_I was evaluated using the photoelastic measurement results by employing the Irwin method [4]. The data necessary to determine K_I were available in the form of isochromatic fringe loops which occur in the region adjacent to the crack tip. The Cartesian components of stress: σ_x, σ_y and τ_{xy} in the neighbourhood of the crack tip were:

$$\sigma_x = \frac{K_I}{\sqrt{2\pi r}}\cos\frac{\Theta}{2}\left(1-\sin\frac{\Theta}{2}\sin\frac{3\Theta}{2}\right)+\sigma_{ox},$$

$$\sigma_y = \frac{K_I}{\sqrt{2\pi r}}\cos\frac{\Theta}{2}\left(1+\sin\frac{\Theta}{2}\sin\frac{3\Theta}{2}\right),$$

$$\tau_{xy} = \frac{K_I}{\sqrt{2\pi r}}\sin\frac{\Theta}{2}\cos\frac{\Theta}{2}\cos\frac{3\Theta}{2}.$$

Irwin [4] has shown that K_I and the far field stress component – σ_{ox} can by determined from a single point measurement on one isochromatic fringe loop. In the point where:

$$\partial\tau_m / \partial\Theta_m = 0,$$

we obtain the followings equation:

$$2\tau_m = \sigma_1 - \sigma_2,$$

from which

$$\sigma_{ox} = \frac{2\tau_m \cos\Theta_m}{\cos(3\Theta_m/2)\cdot\left(\cos^2\Theta_m + \frac{9}{4}\sin^2\Theta_m\right)^{1/2}},$$

and the K_I value can by determined from:

$$K_I = 2\tau_m\sqrt{2\pi\cdot r_m}\, f(\Theta_m), \tag{1}$$

$$f(\Theta_m) = \frac{1}{\sin\Theta_m}\left[1+\left(\frac{2}{3\mathrm{tg}\Theta_m}\right)^2\right]^{-\frac{1}{2}}\cdot\left(1+\frac{2\mathrm{tg}(3\Theta_m/2)}{3\mathrm{tg}\Theta_m}\right),$$

where: r_m and Θ_m – are the polar coordinates whose origin is defined at the crack tip; $2\tau_m = k_\sigma m_i = \sigma_1 - \sigma_2$ – is known from the stress optic relation; k_σ – is material- fringe value and m_i – isochromatic fringe order. An example of the experimental results is presented in Fig. 2. The value of K_I was also determined from [19], [20]

$$K_I = \frac{P\sqrt{a}}{bW}\left[29.6 - 185.5(a/W) + 655.7(a/W)^2 - 1017(a/W)^3 + 638.9(a/W)^4\right].$$

Fracture mechanics parameters corresponding to pure bending.

The four point bending tests were carried out in the experiment. One applied the flexure notched beam test with artificial crack. The fracture energy G_C was determined by the four point bending tests on 6 specimens of size (10×30×250 mm with 1 crack notched on the center line). The notch depth was equal to 10.0mm (a/h = 1/3). The stress intensity factor K_{IC} for the specimens was evaluated from load-deflexion diagram under the ASTM E813-81 standard. The photoelastic measurement results were taken into account by employing [4]. A good approximation of g_b and g_t in the range of $0<\xi<0.7$ was obtained by using the boundary collocation analysis presented in [5], with the result

$$K_I = \frac{M}{b\cdot h^{3/2}} g_b(\xi) \qquad \text{where: } \xi = a/h,$$

$$g_b(\xi) = 6[\xi^{1/2}(1.99 - 2.47\xi + 12.97\xi^2 - 23.17\xi^3 + 24.8\xi^4)].$$

The shearing mode of fracture – Mode II

In view of the observed tendency of Mode II failures to occur under certain condition of loading, and in the absence of any experimental data (for material using in experiment), the Author had to manufacture a specimen suitable for Mode II fracture testing and to analyze it.

a) CT - specimen

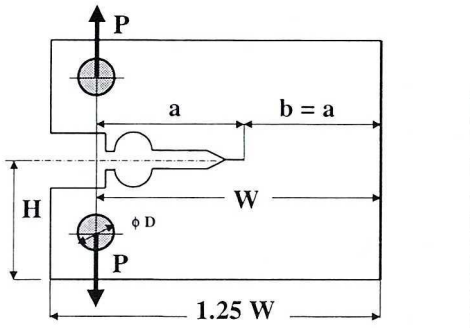

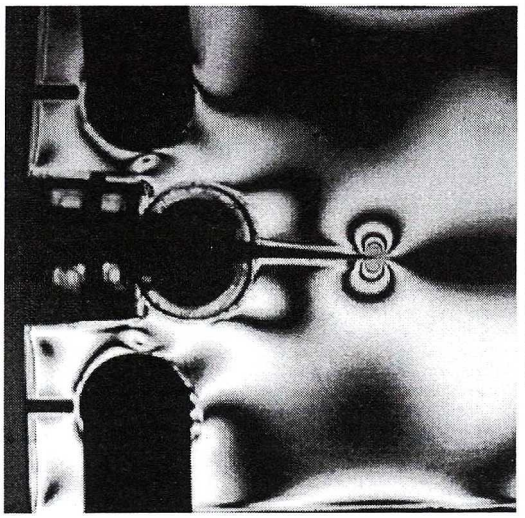

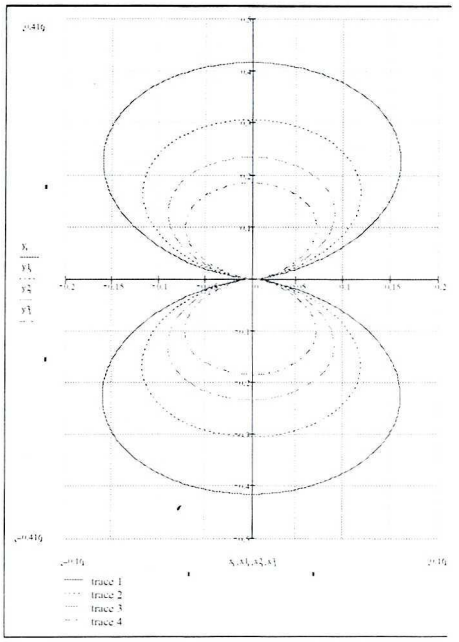

a) CT m=6.0, r_m=2.2mm, Θ_m=104°, f(Θ) =1.09 from (1) K_{IC} =1.29 MPa $m^{1/2}$
ASTM – P_c=624 N, ΔG_C = 0.46 kN/m, K_{IC}≅1.34 MPa $m^{1/2}$

K_I = 32.61 MPa $m^{1/2}$; m_z=12, 14, 16, 18; k_σ=1.68 MPa/rz. iz. – principal stresses σ_1 and σ_2

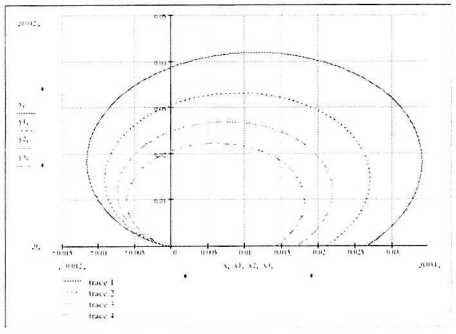

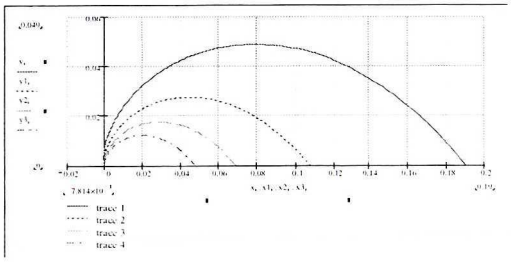

Fig. 2. Fracture mechanics parameters. CT - specimen according to the ASTM E399 and E813-81 standards and isochromatic patterns associated with the crack propagation and the principal stresses σ_1 and σ_2 for m_z = 6, 8, 10, 12

a) m=6, Θ=131.8°, r=2.4mm b) m=8, Θ≅92°, r=1.25mm

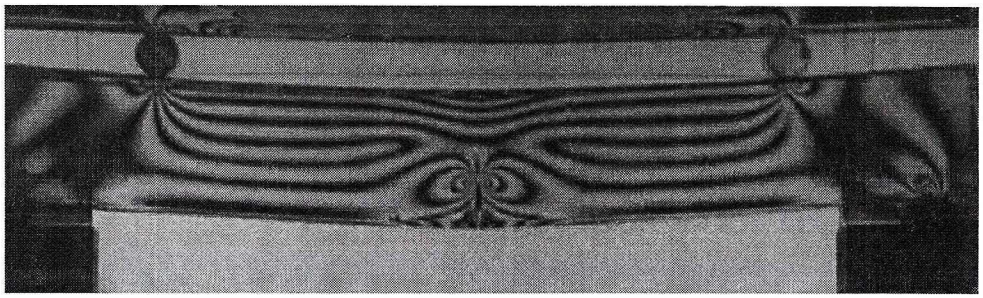

b)

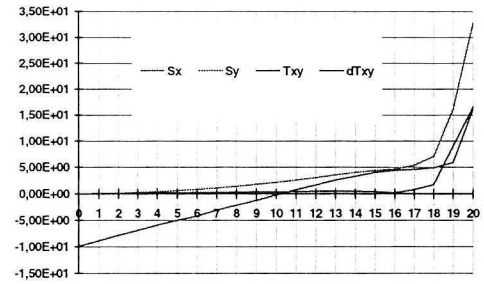

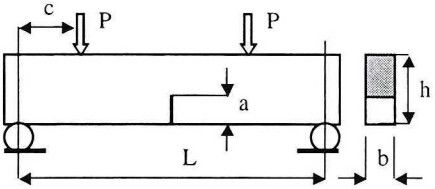

m=8.5, r_m=1.2mm, Θ_m=102°, f(Θ) =1.064, K_{IC} =1.32 MPa $m^{1/2}$

Fig. 3. a) Fracture mechanics parameters corresponding to pure bending and isochromatic patterns associated with the crack propagation, b) Stresses σ_x corresponding to pure bending and typical crack development of the matrix in the tension zone.

The stress intensity factor K_{IIC} was evaluated from the load-displacement curve using the compact shear specimen CS and the beam subjected to asymmetric loading shown in Figure 5 and by applying the photoelastic measurement results and the Wiliams stress function [24]. The Cartesian components of stress: σ_x, σ_y and τ_{xy} in the neighbourhood of the crack tip were:

$$\sigma_x = -\frac{K_{II}}{\sqrt{2\pi r}}\sin\frac{\Theta}{2}\left(2+\cos\frac{\Theta}{2}\cos\frac{3\Theta}{2}\right),$$

$$\sigma_y = \frac{1}{\sqrt{2\pi r}}K_{II}\sin\frac{\Theta}{2}\cos\frac{\Theta}{2}\cos\frac{3\Theta}{2}, \qquad (2)$$

$$\tau_{xy} = \frac{1}{\sqrt{2\pi r}}K_{II}\cos\frac{\Theta}{2}\left(1-\sin\frac{\Theta}{2}\sin\frac{2\Theta}{2}\right),$$

from which $2\tau_m = K_{II}\sqrt{\frac{1}{2\pi r}(4\cos^2\Theta+\sin^2\Theta)}$,

and the K_{II} value can by determined from:

$$K_{II} = 2\tau_m\sqrt{2\pi r/(4\cos^2\Theta+\sin^2\Theta)}. \qquad (3)$$

Two examples of the experimental results are presented in Figs. 4 and 6.

For the compact shear specimen CS, K_{IIC} value was also determined from [4], [7], [8]

$$K_{II} = \frac{P}{BH} F_{II} \sqrt{a} .$$

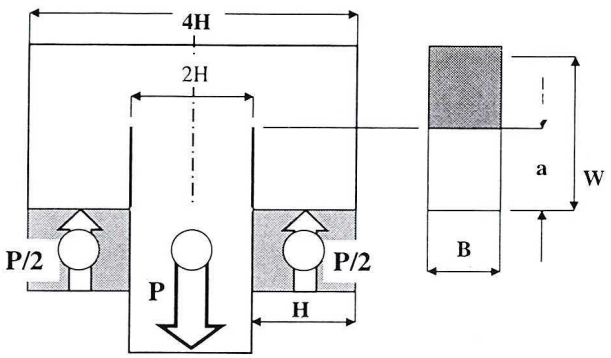

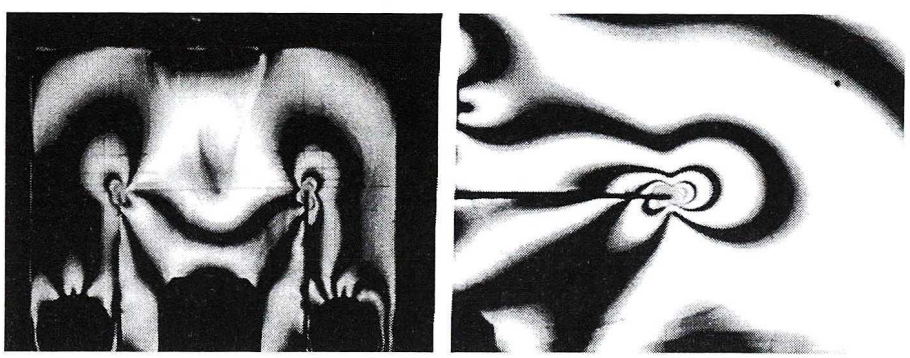

m=17.5.5, r_m=1.25mm, Θ_m=0°, k_σ=1.68 MPa/fr and from (3) K_{IC} =1.30 MPa $m^{1/2}$

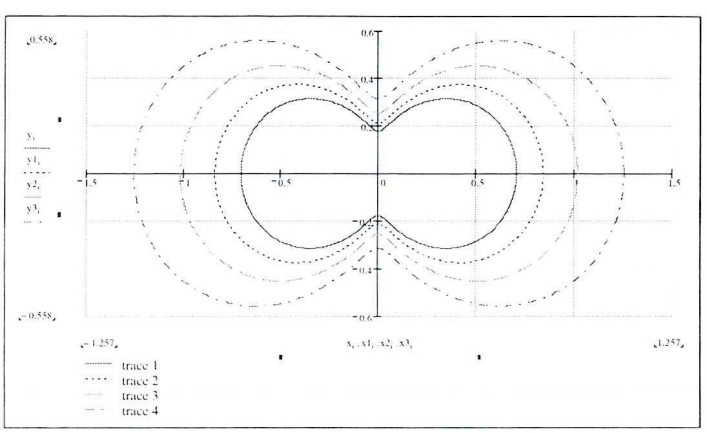

K_{II} = 1.34 MPa·$m^{1/2}$

Fig.4. Compact shear specimen CS and isochromatic patterns for a load P=95 N, K_{IIC} value was determined from (3) and (4) for a load P_c=177.5 N and a/W=0.5, K_{IIC}=1.39 MPa·$m^{1/2}$

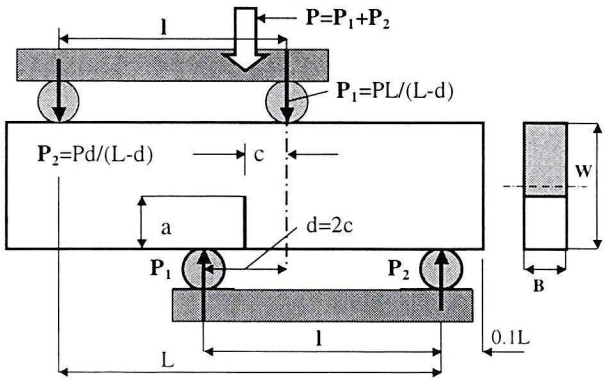

Rys.5. The beam subjected to asymmetric loading

a)

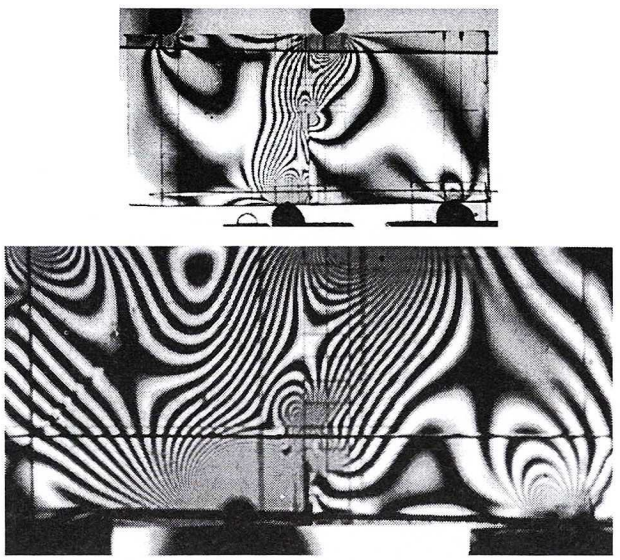

b)

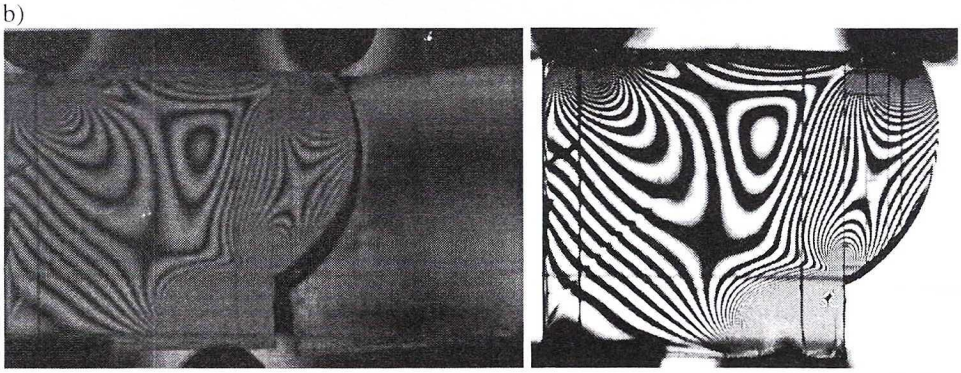

Fig. 6. The beam subjected to asymmetric loading and isochromatic patterns associated with the crack propagation, a) before cracking b) just (1/250 sec.) after cracking for a load P_c=1220 N and a/W=0.3, K_{IIC}=1,45 MPa $m^{1/2}$

For the beam subjected to asymmetric loading (Fig. 6) K_{IIC} was evaluated by applying the photoelastic method [3], [4] from (3) and from $K_{II} = \frac{Q}{B\sqrt{W}} F^{II}(a/W)$ where $Q=P_1-P_2$ and also for comparison from [20]

$$K_{II} = \frac{2Q}{\sqrt{\pi a}}\left[1.3-0.65\left(\frac{a}{W}\right)+0.37\left(\frac{a}{W}\right)^2+0.28\left(\frac{a}{W}\right)^3\right]\frac{1}{\sqrt{1-\left(\frac{a}{W}\right)}}.$$

2.2. The photoelastic models of the reinforced composites

The models were manufactured in the same way as the element of reinforced composite using cold casting of epoxy resin "Ep-53" (matrix). The element was reinforced by the copper bars, cevlar and carbon fibbers. The models of the reinforced beams were tested in pure bending especially in the cracked stage up to their collapse. It was decided to test a series of beams, to investigate the ultimate limit state corresponding to cracking of the matrix and the plastic deformation or the yield limit of the reinforcement. The state of stress in the matrix, according to the vertical and horizontal crack propagation, was observed using a photoelastic method. The strains in the reinforcement were determined using strain gauges 1.0 mm of length. One determined the critical value of the strain energy release rate ($G_C=\partial U/\partial A$) obtained experimentally from the relation between the work of the acting forces and the crack surface. In the case of vertical propagation of cracks, which develop directly (perpendicularly to the beam axis), the displacements of the forces and the propagation of the crack in the matrix corresponding to them allows us to determine the stress intensity factor K_{IC} and the strain energy release rate G_{IC} from:

$$G_{IC} = \frac{\Delta U}{\Delta A} = \frac{P_i \Delta V_i}{aB}; \quad \text{and} \quad K_{IC} = \sqrt{E_m \cdot G_{IC}}, \tag{4}$$

where: ΔU – dissipated energy, $\Delta A = aB$ – fractured area, P_i – force corresponding to the crack propagation, ΔVi – displacement corresponding to the cracks length (a).

3. Cracking mechanisms

3. 1. Crack propagation vertical - perpendicular to the beam axis

For computation of the ultimate moment M_{CR} related to the crack propagation, the strain energy release rate G_C was evaluated based on the known isotropic linear elasticity solution.

The critical load causes the propagation of cracks, which develop directly, perpendicular to the beam axis. For simplification (shown in Fig. 7), the linear stress distribution in the matrix was assumed. According to the theory of strength of materials, the stresses in reinforced beams can be easily calculated.

The stress intensity factor K_I for the specimens was evaluated based on the known isotropic linear elasticity solution. From dimensional consideration, the stress intensity factor $K_I^{(M)}$ depends upon the applied bending moment M_a, and axial force Z_a in the reinforcement is related to the stress intensity factor $K_I^{(Z)}$. The stress intensity factor K_I is given by the superposition principle:

$$K_I = K_I^{(M)} + K_I^{(Z)} \tag{5}$$

$$K_I^{(M)} = \frac{M_a}{b \cdot h^{3/2}} g_b(\xi) \qquad K_I^{(Z)} = \frac{Z}{b \cdot h^{1/2}} g_t(\xi) \qquad \text{where: } \xi = a/h \tag{6}$$

A good approximation of g_b and g_t for the range of $0 < \xi < 0.7$ can obtained by using the boundary collocation analysis presented in [5], [12] with the result

$$\begin{aligned} g_b(\xi) &= 6\left[\xi^{1/2}(1.99 - 2.47\xi + 12.97\xi^2 - 23.17\xi^3 + 24.8\xi^4)\right] \\ g_t(\xi) &= \xi^{1/2}(1.99 - 0.41\xi + 18.7\xi^2 - 38.48\xi^3 + 53.85\xi^4) \end{aligned} \tag{7}$$

The applied bending moment M_a and axial force Z produce local rotations, respectively:

$$\Phi^{(M)} = \lambda_{MM} \cdot M_a, \qquad \Phi^{(Z)} = \lambda_{MZ} \cdot Z_a, \tag{8}$$

where: $\lambda_{MM} = \frac{2}{bh^2 E_m} \int_0^{\xi} g_b^2(\xi) d\xi, \qquad \lambda_{MZ} = \frac{2}{bhE_m} \int_0^{\xi} g_t g_b(\xi) d\xi .$

Up to the moment of nonlinear deformations of the reinforcement, the local rotation in the cracked cross-section is equal to zero:

$$\Phi = \Phi^{(M)} + \Phi^{(Z)} = 0 . \tag{9}$$

The bending moment M_a (in cracked section) depends upon the applied bending moment M and axial force Z_a in the reinforcement.

$$M_a = M - Z_a(h/2 - e_0),$$

and from (7) and (8)

$$\begin{aligned} \lambda_{MM}\left[M - Z_a(h/2 - e_0)\right] - \lambda_{MZ} \cdot Z_a = 0, \\ M = Z_a\left[(h/2 - e_0) + h \cdot r(\xi)\right], \end{aligned} \tag{10}$$

where: $h \cdot r(\xi) = \lambda_{MZ} / \lambda_{MM}$, λ_{MM} and λ_{MZ} are determined from (8).

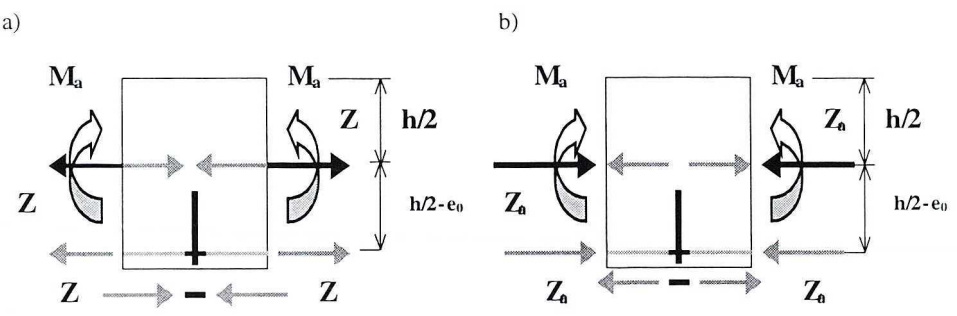

Fig. 7. Cracked reinforced beam element and axial force Z_a in reinforcement: a) - axial force in the reinforcement causes the propagation of cracks, b) – tensile axial force $\mathbf{Z_a = -Z}$ in the reinforcement actually restrains the cracks

In the case of nonlinear deformations of the reinforcement, the stress intensity factor K_I of crack propagation can by found from (5):

$$K_I = \frac{g_h(\xi)}{bh^{3/2}}\left[M - Z_a \cdot (h/2 - e_0)\right] - \frac{Z_a}{bh^{1/2}} g_t(\xi) \tag{11}$$

where: $Z_a = -Z$.

In the case of completely open crack, the local rotation in the cracked cross-section equals

$$\Phi^{(M)} + \Phi^{(Z)} = \Phi^{(M_{CR})},$$

$$\lambda_{MM}\left[M - Z_a(h/2 - e_0)\right] + \lambda_{MZ} Z = \lambda_{MM} M_{(K_{IC})},$$

where: $Z = -Z_a$, $M_{(K_{IC})} = K_{(IC)} \dfrac{bh^{3/2}}{g_h(\xi)}$.

The moment corresponding to the crack propagation is:

$$M_{CR} = K_{IC} \frac{b \cdot h^{3/2}}{gb(\xi)} + Z_a \left[\left(\frac{h}{2} h/2 - e_0\right) + \frac{\lambda_{MZ}}{\lambda_{MM}}\right], \tag{12}$$

where:

- $Z_a = \varepsilon_r E_r F_r$ for $\varepsilon \le \varepsilon_0$ and for $\varepsilon_r \rangle \varepsilon_0$ $Z_a = \sigma(\varepsilon_r) F_r$ and $\sigma(\varepsilon_r) = \sigma(\varepsilon_r/\varepsilon_O)^p$,
- p=0.072 (obtained experimentally), F_r – cross section of the reinforcement,
- strains (ε_r) in the reinforcement were determined using strain gauges 1.0 mm of length.

The displacement in the crack may by derived by local rotation in the cracked cross-section and crack length **a** as the crack opening displacement (COD)

$$\delta_{(a)} = \Phi^{(CR)} \cdot a. \tag{13}$$

The corresponding axial displacement of the reinforcement $\delta(Z)$:

$$\delta_{(Z)} = \Phi^{(CR)} \cdot (a - e_0) = \lambda_{MM} M_{(K_{IC})} \cdot (a - e_0). \tag{14}$$

Applying the critical value of K_{IC} of the matrix and the crack length "a" and the strains of the reinforcement, one obtains the ultimate moment (M_{CR}). The bending moment M_{CR} for 3 different percentage values of the reinforcement (2%, 1%, 0%), in the case of vertical cracking, is presented in Fig. 8.

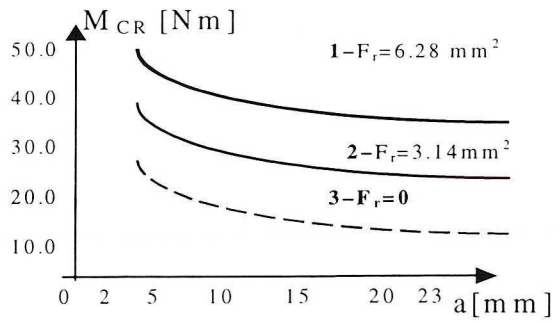

Fig. 8. The values of the ultimate moment (M_{CR}) in the case of vertical cracking

Experimental and numerical results of the limit state

Table 1.

Ultimate moment M_{CR} corresponding to vertical crack propagation
h = 33.5 mm, K_{IC}=1.31 MPa·m$^{1/2}$, e_0=4.5mm, σ_0=188 MPa, ε_0=0.002

a [mm]	$\varepsilon_r \cdot 10^3$	Z_a [N]	M_a [Nm]	M_{CR} [Nm]	$\Phi \cdot 10^{-3}$ [rd]	$\delta(a)$ [mm]	M_{CR}-Exp [Nm]
2.0	2.4	1196	29.131	50.962	0.686	$1.37 \cdot 10^{-3}$	-
5.0	3.6	1232	18.810	42.260	2.65	$13.3 \cdot 10^{-3}$	-
10.0	21.0	1398	12.341	41.005	8.09	$80.9 \cdot 10^{-3}$	39.5
15.0	35.0	1451	8.347	40.510	17.9	0.269	40.4
20.0	42.0	1470	5.168	40.437	3.86	0.773	43.2
23.0	44.0	1475	3.662	40.427	6.27	1.44	44.5
Horizontal cracks propagation – parallel to the beam axis							

3.2. Horizontal cracks propagation - parallel to the beam axis.

Some simplifications in theoretical analysis are based on experimental observations. The critical load causes propagation of the cracks that have developed directly, perpendicular to the beam axis, but further, as the load increases, they turn and run parallel to the beam axis. The crack path in the second stage of the crack propagation, when it is running almost parallel to the beam axis, can by influenced by the changes of mechanical conditions (compressive zone) at the end of the beam. The stress intensity factors K_I and K_{II} can be calculated from the J-integral by using the theory of strength of materials (for simplified model shown in Fig. 9).

$$J = \int_s (\tfrac{1}{2}\sigma_{ij}\varepsilon_{ij}dx_2 - T_i^n \frac{\partial u_i}{\partial x_1} ds) = \frac{1}{2E_m}[\int_{S1} \sigma_x^2 ds_1 - \int_{S3} \sigma_x^2 ds_3 + \int_{S5} \sigma_x{}^2 ds_5] \qquad (15)$$

This approach is justified because fracture initiation experiments show linear behaviour near cracks in these (composite) specimens.

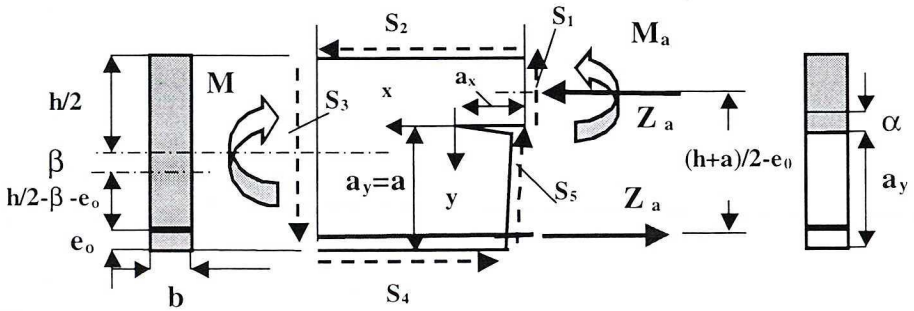

Fig. 9. Internal forces over cross section corresponding to cracking parallel to the beam axis

Let us consider a short section, loaded by the stress-resultants M and Z_a that contains a quasistatically propagating horizontal crack (parallel to the beam axis). In the model shown in Fig. 10, the stress intensity factors K_I and K_{II} can be found by using the theory of strength of materials assuming linear stress distribution in the matrix. For both loading cases, the crack is predominately loaded by in-plane shear, so we can assume that:

$$K_{II} = \sqrt{E \cdot J_H}, \quad K_I = \sqrt{E \cdot J_B} \quad \text{and} \quad J = J_B + J_H. \tag{16}$$

Assuming linearly elastic stress distribution in the matrix, the J_B –integral describing the bending energy during the mode I loading (cracking by tension) can by determined. Similarly, the integral J_H corresponding to horizontal shear forces Z_a can by evaluated. The results are as follows:

$$J_B = \frac{6}{E_m b^2}\left[\frac{M_a^2}{(h-a)^3} - (M - Z_a \cdot h/2)^2 \cdot \frac{1}{h^3} + \frac{Z_a^2}{a^3}(a/2 - e_0)^2\right],$$
$$J_H = \frac{Z_a^2}{E_m b^2}\left[\frac{1}{2}\left(\frac{1}{h-a} + \frac{1}{a}\right) - \frac{3}{2h}\right]. \tag{17}$$

A local crack tip stress analysis is essential for fracture under combined loading for both loading modes (I and II). The values of the stress intensity factors K_I and K_{II} can be found from the strain energy release rate G_C and G_I and G_{II} corresponding to pure mode I and pure mode II. Assuming that the axial forces in the reinforcement in the cracked section and uncracked section (Fig. 11) are equal Z_a and Z_l, respectively, the strain energy release rates G_C, G_I and G_{II} can by calculated by using the theory of strength of materials, as follows:

$$K_I = \sqrt{EG_I}, \quad K_{II} = \sqrt{E \cdot G_{II}} \quad \text{and} \quad K_C = \sqrt{E \cdot G_C}, \tag{18}$$

$$G_C = J = \frac{1}{2E_m}\left\{\frac{12M_a^2}{b^2(h-a)^3} - \left(\frac{M_L}{J_L}\right)^2\left[\frac{(h-e_0)^3}{3} - \frac{h(h-e_0)^2}{2} + \left(\frac{h}{2}\right)^2(h-e_0)\right] + \right.$$
$$\left. + \frac{Z_a^2}{b^2(h-a)} - 2\frac{(M_l - M_a)Z_l}{J_l \cdot bh}\left[\frac{(h-e_0)^2}{2} - \frac{h}{2}(h-e_0)\right] + \frac{(M_l - M_a)(Z_l - Z_a)}{3 \cdot b \cdot J_l}\left(\frac{h}{2} - e_0\right)\right\}, \tag{19}$$

$$G_I = \frac{1}{2E_m}\left\{\frac{12M_a^2}{b^2(h-a)^3} - \left(\frac{M_l}{J_l}\right)^2(h-e_0)\left[\frac{(h-e_0)^2}{3} - \frac{h(h-e_0)}{2} + \left(\frac{h}{2}\right)^2\right]\right\}, \tag{20}$$

$$G_{II} = \frac{1}{2E_m}\left\{\frac{Z_a^2}{b^2(h-a)} - \left(\frac{M_l - M_a}{J_l}\right)^2\left[\frac{(h-e_0)^3}{3} - \frac{h(h-e_0)^2}{2} + \left(\frac{h}{2}\right)^2(h-e_0)\right] - \right.$$
$$\left. - 2\frac{(M_l - M_a)Z_l}{J_l \cdot bh}\left[\frac{(h-e_0)^2}{2} - \frac{h}{2}(h-e_0)\right] + \frac{(M_l - M_a)(Z_l - Z_a)}{3 \cdot b \cdot J_l}\left(\frac{h}{2} - e_0\right)\right\},$$

where: $M_a = M - Z_a\left(\frac{h+a}{2} - e_0\right)$, $M_1 = M - Z_1\left(\frac{h}{2} - e_0\right)$,

$$Z_a = \frac{M}{J_a}(a - e_0 + \alpha)nF_r, \quad Z_1 = \frac{M}{J_1}(h/2 - e_0)nF_r,$$

for $\varepsilon = \varepsilon_0$, $n = E_r / E_m$ and for $\varepsilon \geq \varepsilon_0$, $\sigma_r = \sigma_0\left(\frac{\varepsilon_r}{\varepsilon_0}\right)^p$, $n = \frac{\sigma_0 \cdot \varepsilon_r^{p-1}}{E_m \cdot \varepsilon_0^p}$,

$$J_a = \frac{b(h-a)^3}{12} + b(h-a)\left(\frac{h-a}{2} - \alpha\right)^2 + n[J_r + F_r(a + \alpha - e_0)^2],$$

$$\alpha = \frac{\frac{b}{2}(h-2)^2 - nF_r(a - e_0)}{b(h-a) + nF_r},$$

$$J_a = \frac{b(h-a)^3}{12} + b(h-a)\left(\frac{h-a}{2} - \alpha\right)^2 + n\left[J_r + F_r(a + \alpha + e_0)^2\right],$$

$$\beta = \frac{(h/2 - e_0)nF_r}{bh + (n-1)F_r},$$

α, β – position of the neutral axis of cracked and uncracked section, respectively,

J_a, J_L, – moments of inertia of cracked section and uncracked section (Fig. 10), respectively,

J_r – moment of inertia of the reinforcement,

F_r – cross section of the reinforcement.

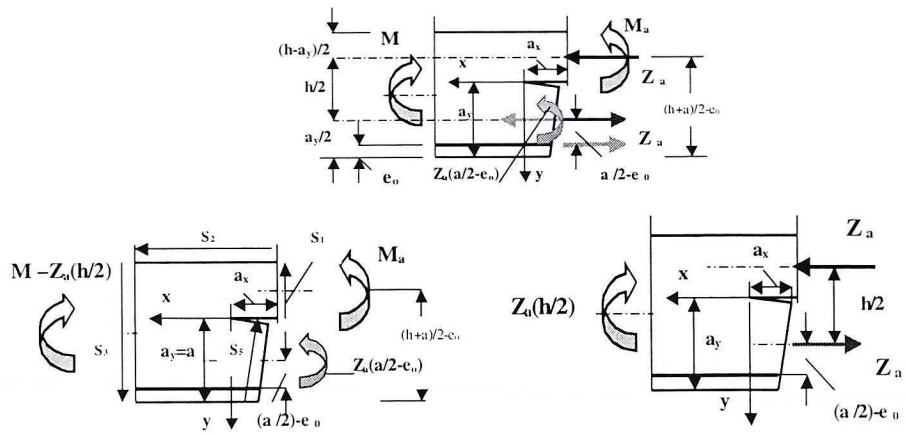

Fig. 10. Internal forces under combined loading in mode I and mode II corresponding to cracking parallel to the beam axis

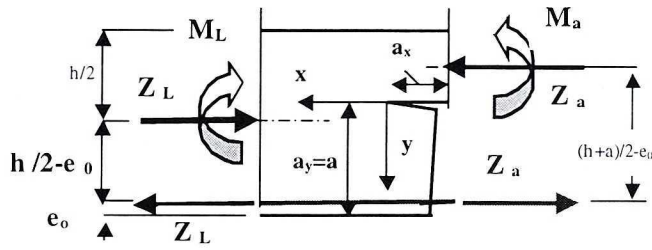

Fig. 11. Internal forces over cracked and uncracked cross sections, respectively

In a general case, the Cartesian components of stress: σ_x, σ_y and τ_{xy} in the neighbourhood of the crack tip are:

$$\sigma_x = \frac{1}{\sqrt{2\pi r}}\left[K_I \cos\frac{\Theta}{2}\left(1-\sin\frac{\Theta}{2}\sin\frac{3\Theta}{2}\right)-K_{II}\sin\frac{\Theta}{2}\left(2+\cos\frac{\Theta}{2}\cos\frac{3\Theta}{2}\right)\right]+\sigma_{ox},$$

$$\sigma_y = \frac{1}{\sqrt{2\pi r}}\left[K_I \cos\frac{\Theta}{2}\left(1+\sin\frac{\Theta}{2}\sin\frac{3\Theta}{2}\right)+K_{II}\sin\frac{\Theta}{2}\cos\frac{\Theta}{2}\cos\frac{3\Theta}{2}\right], \qquad (21)$$

$$\tau_{xy} = \frac{1}{\sqrt{2\pi r}}\left[K_I \sin\frac{\Theta}{2}\cos\frac{\Theta}{2}\cos\frac{3\Theta}{2}+K_{II}\cos\frac{\Theta}{2}\left(1-\sin\frac{\Theta}{2}\sin\frac{2\Theta}{2}\right)\right],$$

from which:

$$(\sigma_1-\sigma_2)^2 = \frac{1}{2\pi r}\left[(K_I \sin\Theta+2K_{II}\cos\Theta)^2+(K_{II}\sin\Theta)^2\right]-$$
$$2\frac{\sigma_{ox}}{\sqrt{2\pi r}}\sin\frac{\Theta}{2}\left[K_I \sin\Theta(1+2\cos\Theta)+K_{II}(1+2\cos^2\Theta+\cos\Theta)\right]+\sigma_{ox}^2 \qquad (22)$$

By inserting the values $k_\sigma = m_i = \sigma_1-\sigma_2$ into (22) we obtain the isochromatics curves in polar coordinates (r, Θ). For each isochromatic loop, the position of maximum angle Θ_m corresponds to the maximum radius of the r_m. This principle can also be used in the mixed mode analysis [11] by employing information from two loops in the near field of the crack, if the far field stress component – $\sigma_{ox}(\Theta)=\text{const}$. Differentiating Eqn (22) with respect to Θ, setting $\Theta=\Theta_m$ and $r=r_m$ and using Eqn $(\partial\tau_m/\partial\Theta_m=0)$ gives:

$$f(K_I,K_{II},\sigma_{ox}) = \frac{1}{2\pi r_m}\left[(K_I \sin\Theta_m+2K_{II}\cos\Theta_m)^2+(K_{II}\sin\Theta_m)^2\right]-$$
$$2\frac{\sigma_{ox}}{\sqrt{2\pi r r_m}}\sin\frac{\Theta_m}{2}\left[K_I \sin\Theta_m(1+2\cos\Theta_m)+K_{II}(1+2\cos^2\Theta_m+\cos\Theta_m)\right]+ \qquad (23)$$
$$+\sigma_{ox}^2-(k_\sigma\cdot m)^2=0,$$

$$g(K_I, K_{II}, \sigma_{ox}) = \frac{1}{2\pi r}\left[K_I^2 \sin 2\Theta_m + 4K_I K_{II} \cos 2\Theta_m\right] -$$

$$-2\frac{\sigma_{ox}}{\sqrt{2\pi r}} \sin\frac{\Theta_m}{2}\left\{\left[K_I(\cos\Theta_m + 2\cos 2\Theta_m) - K_{II}(2\sin 2\Theta_m + \sin\Theta_m)\right] + \right. \quad (24)$$

$$\left. + \frac{1}{2}\cos\frac{\Theta_m}{2}\left[K_I(\sin\Theta_m + \sin 2\Theta_m) + K_{II}(2 + \cos 2\Theta_m + \cos\Theta_m)\right]\right\} = 0.$$

Substituting the radii r_m and the angles Θ_m from these two loops into a pair of equations of the form given in eqn (24) gives two independent relations dependent on the parameters K_I, K_{II} and σ_{ox}. The third equation is obtained by using Eqn (23). The three equations obtained in this way have the form

$$\begin{aligned} g_i(K_I, K_{II}, \sigma_{ox}) &= 0, \\ g_j(K_I, K_{II}, \sigma_{ox}) &= 0, \\ f_k(K_I, K_{II}, \sigma_{ox}) &= 0. \end{aligned} \quad (25)$$

In order to determine K_I, K_{II} and σ_{ox} it is sufficient to select two arbitrary points r_i, Θ_i and apply the Newton-Raphson method to the solution of three simultaneous non-linear equations (25). Example of the numerical results obtained from (25):

For r_1=0.35mm, Θ_1=0.695 rd, m_1=12.0 fr, r_2=0.92 mm, Θ_2=0.642 rd.

we hawe K_I=0.584 MPa $m^{1/2}$, K_{II}=-1.27 MPa $m^{1/2}$ and σ_{ox}=0.02 MPa.

After assuming that in the neighbourhood of the crack tip the far field stress component – σ_{ox}=0, the followings equations are obtained:

$$\tau_m = \sqrt{\left(\frac{\sigma_x - \sigma_y}{2}\right)^2 + \tau_{xy}^2},$$

$$\tau_m = \sqrt{\frac{1}{2\pi r}\left[\left(K_I \sin\Theta_m + 2K_{II}\cos\Theta_m\right)^2 + \left(K_{II}\sin\Theta_m\right)^2\right]}. \quad (26)$$

This equation may by used to construct the isochromatics loops for curves of constant stress τ_{max}. Inserting the values "$k_\sigma m$" into (26) we obtain the isochromatics curves in polar coordinates (r,Θ) in the neighbourhood of the crack tip

$$r(\Theta) = \frac{(K_I \sin\Theta + 2K_{II}\cos\Theta)^2 + (K_{II}\sin\Theta)^2}{2\cdot\pi(k_\sigma \cdot m)^2}, \quad (27)$$

and the values of the angle Θ_m and radius r_m. corresponding to maximum shear stress τ_{max}.

The angle Θ_m is found by setting $\partial\tau_m / \partial\Theta_m$=0 from (26). The resulting equation is

$$\mathrm{tg}2\Theta_m = -\frac{4K_I K_{II}}{K_I^2 - 3K_{II}^2} \quad \text{and} \quad \left(\frac{K_{II}}{K_I}\right)^C - \frac{4}{3}\left(\frac{K_{II}}{K_I}\right)\mathrm{c\,tg}2\Theta_m - \frac{1}{3} = 0 \quad (28)$$

By inserting the values r_i, Θ_i in three selected arbitrary points into (23) we obtain three non-linear equations (i = 1, 2, 3)

$$f_i(K_I, K_{II}, \sigma_{ox}) = 0 \tag{29}$$

and applying the Newton-Raphson method to the solution we have K_I, K_{II} and σ_{ox}. Example of the numerical results (shown in Fig. 12) obtained from (29):

for r_1=0.69 mm, Θ_1=0.639 rd, m_1=14.5 mm, r_2=0.98 mm, Θ_2=0.643 rd. m_2=10.4, r_3=1.18 mm, Θ_3=0.656 rd, m_3=6.5,

we hawe K_I= 1.27 MPa $m^{1/2}$, K_{II} = -0.841 MPa $m^{1/2}$ and σ_{ox}=2.472 MPa.

The results of the numerical analysis were verified experimentally by photoelastic investigation. The isochromatics-fringe patterns obtained under the loading condition corresponding to cracking parallel to the beam axis, recorded photographically, are shown in Fig. 12. Comparison between the numerical and experimental investigation is presented in tables 2–4. The difference between the analytically predicted isochromatics-fringe patterns distribution and those determined photoelasticaly is less then 5÷6 percent. The initial assumption of linear stress distribution in the matrix for calculation the intensity factors K_I and K_{II} from (16) or (19) caused the errors of about 3÷6 percent.

M_a=5.168 Nm, Z_a= 420 N, a_x=6, h=33.5mm, a_y=23.5mm, b=10mm, h=33.5mm, m=16,18,20,22; K_1 =1.27 MPa $m^{1/2}$, K_2 = -1.03 MPa $m^{1/2}$

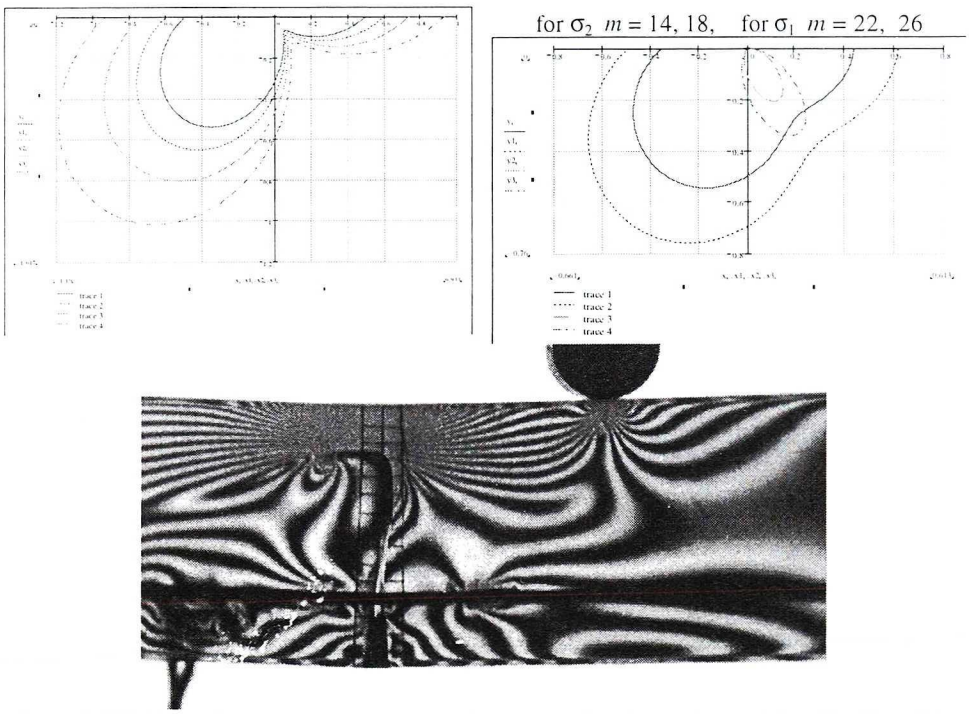

Fig. 12. MODEL L-01. Comparison between the numerical and experimental investigation. The isochromatic patterns σ_1-σ_2 distribution corresponding to typical crack development – parallel to the beam axis propagation

3.3. The strain energy release rate G_C corresponding to horizontal cracks propagation

According to the classical solution, the strain energy release rate G can be found from the following expression:

$$G = G_I + G_{II} = \frac{1}{E_m}\left(K_I^2 + K_{II}^2\right) \tag{30}$$

For a crack horizontal – parallel to beam axis, the local crack tip stress analysis is essential in the fracture problem under combined loading in both mode I and mode II. In pure mode I, one could postulate a K_{IC} condition of fracture.
K_{IC} =1.3÷1.45 MPa $m^{1/2}$, K_{IIC}=1.25÷1.35 MPa $m^{1/2}$, and $c=K_{IC}/K_{IIC} \cong 1.0$.
The values of the strain energy release rate G_I corresponding to pure mode I can be found from:

$$G_{IC} = \frac{K_{IC}^2}{E}. \tag{31}$$

If one assumes $K_{IIC}=K_{IC}$, we have $G_{IIC}=G_{IC}$ for combined loading in both mode I and mode II, the strain energy release rate G_I of the matrix is regarded as a linear function of the G_{II}, $G_I = f(G_{II})$.

$$G_{IC} = G_{IC}\frac{G_{IC}}{G_{IIC}} \cdot G_{II} \quad \text{or} \quad G_I = \frac{K_{IC}^2}{E_m} - \left(\frac{K_{IC}}{K_{IIC}}\right)^2 \cdot G_{II}, \tag{32}$$

from which one obtains an elliptical curve fit of the form

$$\frac{K_I^2}{K_{IC}^2} + \frac{K_{II}^2}{K_{IIC}^2} = 1 \tag{33}$$

and by means of the critical values K_{IC} and K_{IIC} of the matrix, K_I and K_{II} (from an analytical solution or from experience) one obtains the critical values the strain energy release rate G_C and the stress intensity factor K_C for combined loading in both mode I and mode II. An example based on experimental results is presented in Fig. 13b. The stress intensity factors K_{II}, K_I and K_C obtained from (16) are presented in tables 2–4 and those form (19) are presented in tables 5–7 and in Fig. 13a. In this case, the strain energy release rate G_C^{EXP} from the experimental results can be found as follows [25]

$$\left(G_C^{EXP}\right)^2 = G_I^2 + G_{II}^2. \tag{34}$$

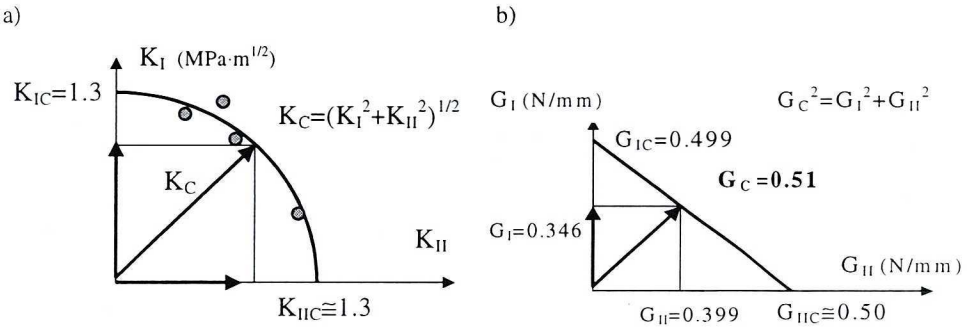

Fig. 13. a) The values of the K_I, K_{II} of the matrix as a function of the critical values K_{IC} and K_{IIC}; b) The values of the strain energy release rate $\mathbf{G_I}$ and $\mathbf{G_{II}}$ of the matrix as a linear function of the G_{II} obtained from (34) according to mixed mode of the fracture

Numerical and Experimental Results – Horizontal cracks propagation – parallel to the beam axis G_I, G_{II}, G_C, K_I and K_{II} obtained from (16) and (17)

Table 2.

h=31 mm, a=25 mm, e_0=8.0 mm, M = 34.20 Nm, ε_i=0.0035, ε_r=0.0095, Ma=0.658 Nm, Za=1677 N						
G_I	G_{II}	G_C	G_C^{EXP}	K_I	K_{II}	$K(G_C)$
kN/m				MPa·m$^{1/2}$		
0.0591	**0.4488**	0.5079	0.598	0.4515	1.244	**1.324**

Table 3.

h=33.5 mm, e_0=4.5 mm, Mg = 45.20 Nm, ε_i=0.0045, ε_r= 0.0285, M_a=4.641 Nm, Z_a=1690 N						
G_I	G_{II}	G_C	G_C^{EXP}	K_I	K_{II}	$K(G_C)$
kN/m				MPa·m$^{1/2}$		
0.3704	0.2127	0.5831	**0.427**	1.1305	0.857	**1.418**

Comparison between the numerical and experimental investigation

Table 4.

N° point	r_i [mm]	m_i fr.	Θ_i Rd.	Θ_i Deg. °	σ_{ox}	K_i MPa·m$^{1/2}$
1	0.69	14.5	0.638	36.55		K_I =1.165
2	0.98	10.5	0.643	36.84	σ_{ox}=2.01 MPa	K_{II} = -0.791
3	1.18	7.5	0.656	37.60		**K_C = 1.41**

Table 5.

h=36.4 mm, a=23 mm, M=48.5 Nm, ε_i=0.0054, ε_r=0.0192, e=7.5mm, M_a=7.99 Nm, Z_a=1804.5 N						
G_I	G_{II}	G_C	G_C^{EXP}	K_I	K_{II}	$K(G_C)$
kN/m				MPa·m$^{1/2}$		
0.5067	0.1709	0.6775	**0.535**	1.3221	0.768	**1.529**

Numerical and Experimental Results - Horizontal cracks propagation – parallel to the beam axis G_I, G_{II}, G_C, K_I and K_{II} obtained from (19)

Table 6.

h=31 mm, a=25 mm, e_0=8.0 mm, M = 34.20 Nm, ε_l=0.0035, ε_r=0.0095, Ma=0.658 Nm, Za=1677 N						
G_I	G_{II}	G_C	G_C^{EXP}	K_I	K_{II}	$K(G_C)$
kN/m				MPa·m$^{1/2}$		
0.0349	**0.4491**	0.4840	**0.598**	0.3471	1.245	**1.292**

Table 7.

Comparison between the numerical and experimental investigation.

N° point	r_i [mm]	m_i fr.	Θ_i Rd.	Θ_i Deg. °	σ_{ox}	K_i MPa·m$^{1/2}$
1	0.69	14.5	0.639	36.61		K_I =1.274
2	0.98	10.4	0.643	36.84	σ_{ox}=2.472 MPa	K_{II} = -0.8469
3	1.18	6.5	0.656	37.60		**K_C = 1.530**

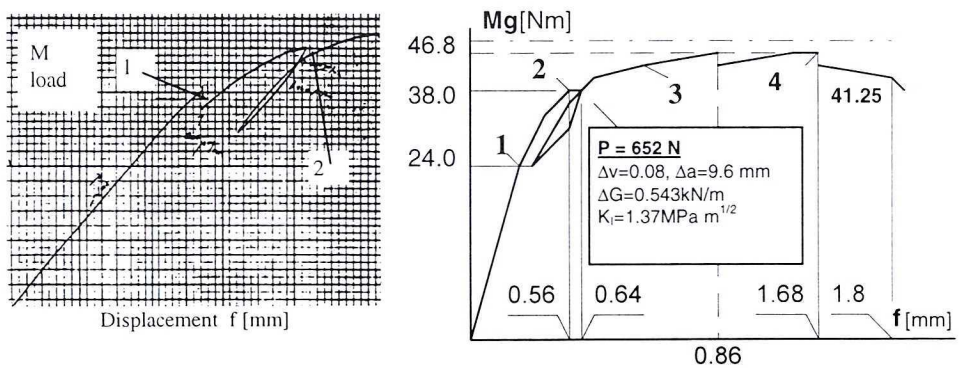

Fig. 14. An example of the load-displacement curve from X-Y plottrer, with characteristic points corresponding to cracking

4. Experimental and numerical investigations of the limit state

The dimensions of the typical model used in the experiment are given in Fig. 1. The models were tested in pure bending especially in the cracked stage. The brittle fracture of the matrix was simulated by introduction of artificially initiated cracks in the tension zone (Fig. 1). The beams were loaded gradually to initiate crack propagation in the matrix and plastic deformation of the reinforcement. The critical load caused propagation of cracks, which developed directly (perpendicularly to the beam axis), but further, as the load increased, turned and run parallel to the beam axis. Test results, isochromatics fringe distribution registered phtoelastically and the force in reinforcement, calculated from the value of strain, allowed us to determine the state of stresses in the cracked stage. The stress distributions related to typical crack development (corresponding to the critical force and the ultimate moment M) are given in Figs. 15 and 16.

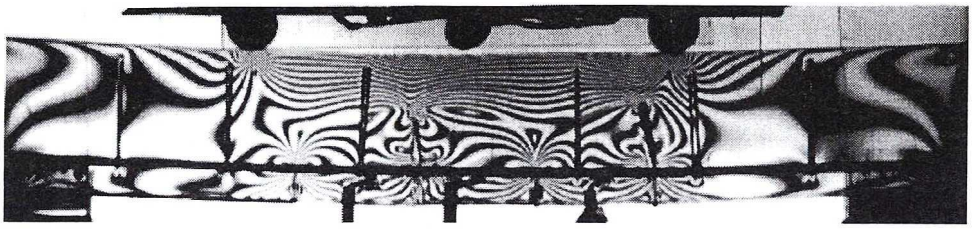

Fig. 15. Photoelastic model of the reinforced beam. The isochromatic distribution patterns (σ_1-σ_2) before vertical cracking

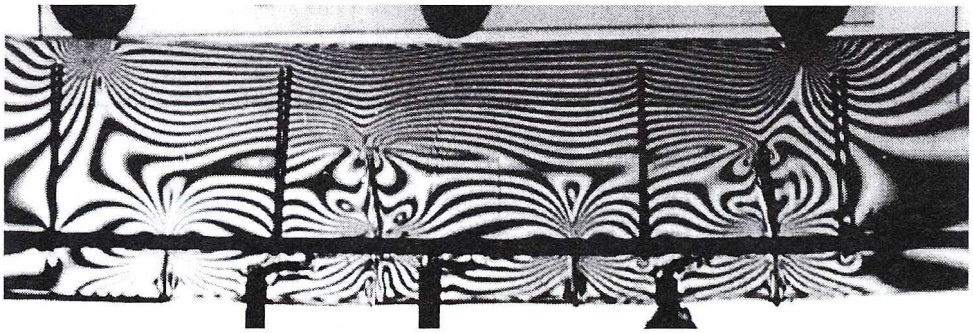

Fig. 16. Photoelastic model of the reinforced beam. The isochromatic distribution patterns (σ_1-σ_2) corresponding to typical crack development – perpendicular the beam axis (point 3 in load-displacement curve – Fig. 18).

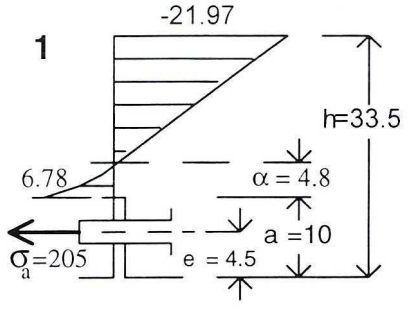

a) P = 690 N, Mg =24 Nm

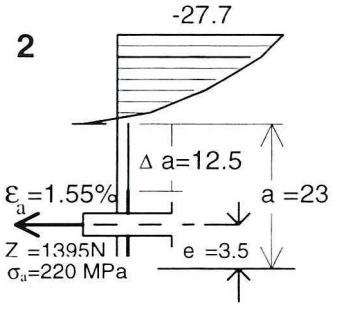

b) P = 690 N, Mg =38 Nm

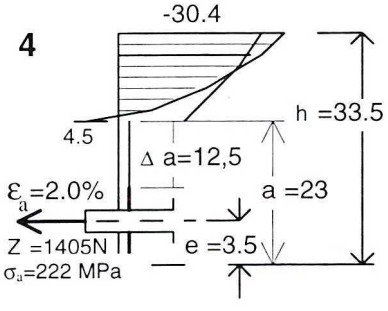

c) P = 810 N, Mg = 44 Nm

Fig. 17. Distribution of stresses σ_x corresponding to perpendicular (a, b) and parallel (c) to the beam axis propagation of the cracks (points 1, 2 and 4 in load-displacement curve in Fig. 18)

a)

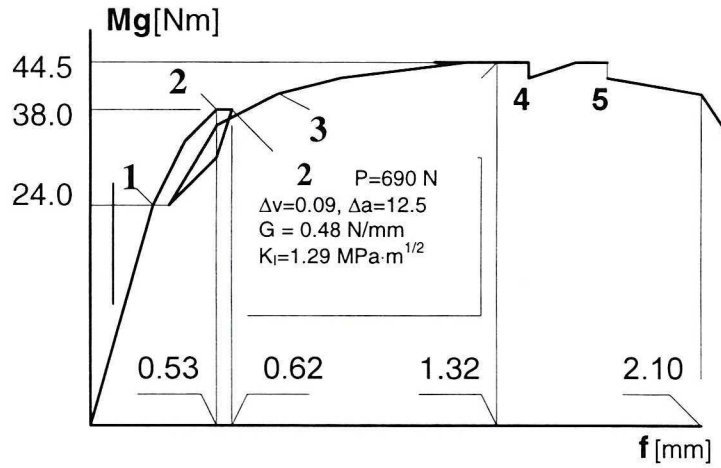

b)

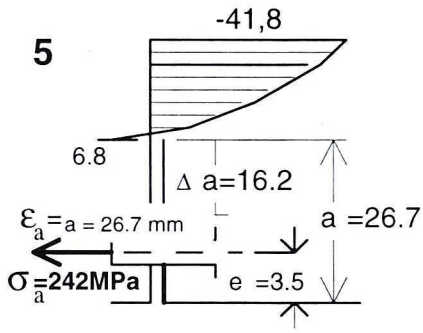

Fig. 18. a) Load-displacement curve; b) Distribution of stresses σ_x corresponding to propagation of the cracks parallel the beam axis (point 5 in load-displacement curve)

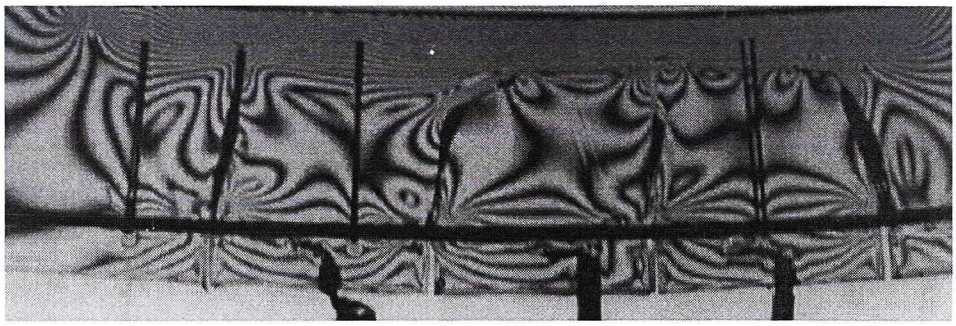

Fig. 19. Fracture in direction parallel to the beam axis. Distribution of isochromatic fringes corresponding to propagation of the cracks parallel to the beam axis (point 5 in load-displacement curve)

5. Numerical determination of stress distribution in the cracked stage

The numerical calculations were carried out using the finite element program ANSYS 5.4 [17], [25] and by applying the substructure technique. Two different methods were used: solid modeling and direct generation. Finite element calculations were performed in order to verify the experimentally observed branching phenomenon and the isochromatic distribution observed during cracks propagation along debonded parts.

The geometry and materials were chosen to correspond to the actual specimens used in the experiments. A finite element mesh of the model (used for numerical simulation) of the structure is presented in Fig. 20, and the stress distribution as well as the isochromatic fringes are shown in Fig. 21. (For comparison, the isochromatics obtained experimentally are given in Fig. 21.) The strain energy release rate G_C is equal in this case to the J-integral:

$$J=\int_s\left\{\frac{1}{2}\left[\frac{1}{E}\left(\sigma_y^2-\sigma_x^2\right)+\frac{\tau_{xy}^2}{2G}\right]\cdot n_1-\left[\frac{\tau_{xy}}{E}\left(\sigma_x-\nu\cdot\sigma_y\right)\cdot n_2+\left(\tau_{xy}n_1+\sigma_y n_2\right)\frac{\partial v}{\partial x}\right]\right\}ds \quad (35)$$

or can by determined from numerical calculation using the finite element method:

$$J=\sum_i\left\{\frac{1}{2}\left[\frac{1}{E_i}\left(\sigma_{yi}^2-\sigma_{xi}^2\right)+\frac{\tau_{xyi}^2}{2G}\right]\cdot n_{1i}-\left[\frac{\tau_{xyi}}{E}\left(\sigma_{xi}-\nu\sigma_{yi}\right)\cdot n_{2i}+\left(\tau_{xyi}n_{1i}+\sigma_{yi}n_{2i}\right)\frac{\Delta v_i}{\Delta x_i}\right]\right\}\cdot\Delta S_i \quad (36)$$

The distribution of the stresses and displacement obtained by FEM allows us to evaluate the J– integral (equal to the strain energy release rate G_C).

a)

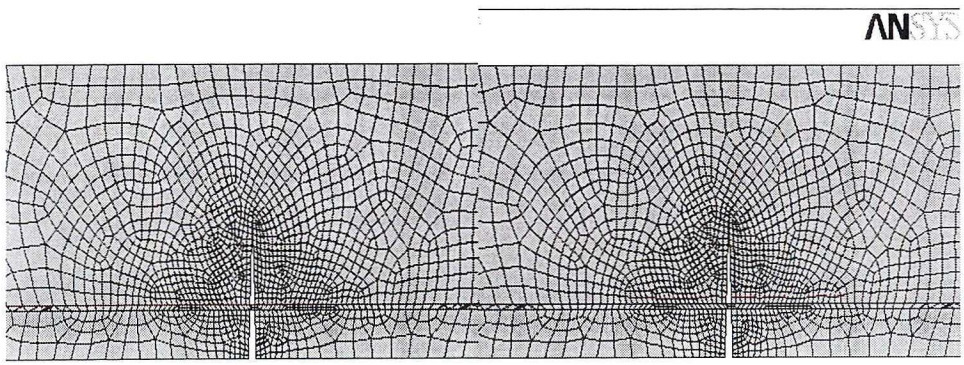

b)

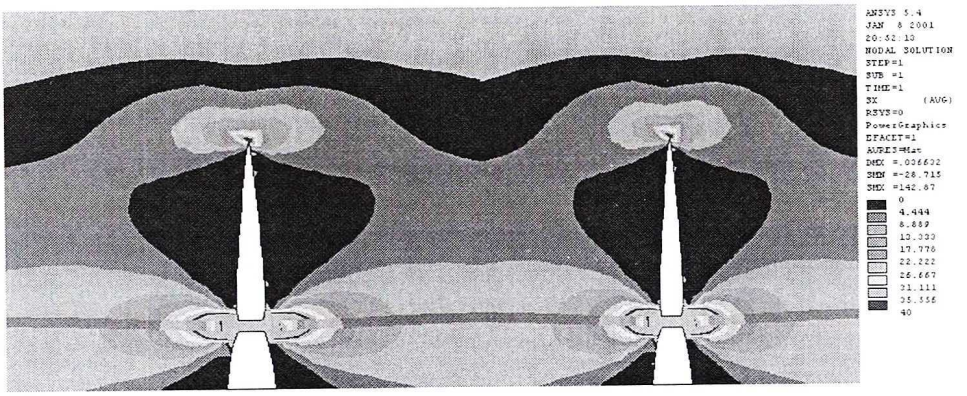

Fig. 20. Numerical simulation of the cracking. Fracture in the direction perpendicular to the beam axis; a) Finite element mesh. b) Distribution of the stresses σ_x,.

5.1. Fracture in direction perpendicular to the beam axis

The J– integral obtained by FEM (equal the strain energy release rate G_C):
$J_{IC} \equiv 0.493 kN/m$, $K_{IC} \equiv (E_m \cdot J)^{1/2} = 1.304\ MPa \cdot m^{1/2}$

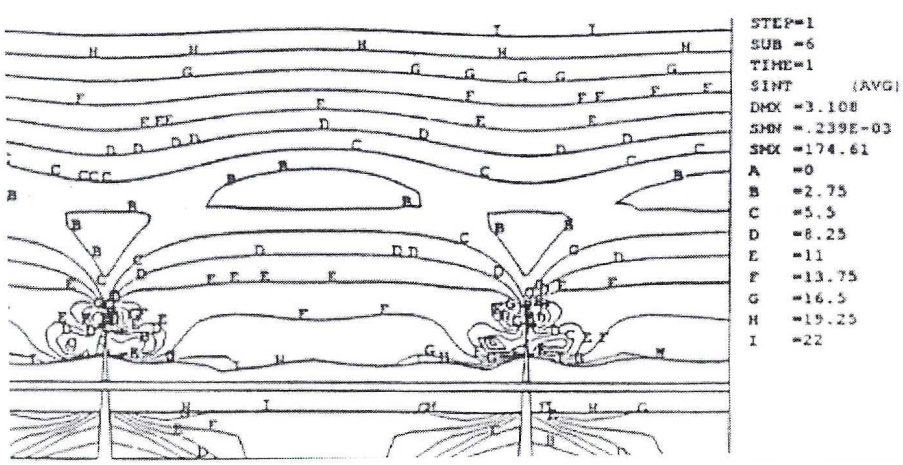

Fig. 21. Distribution of isochromatic fringes (σ_1-σ_2) corresponding to the crtical load before the propagation of the cracks

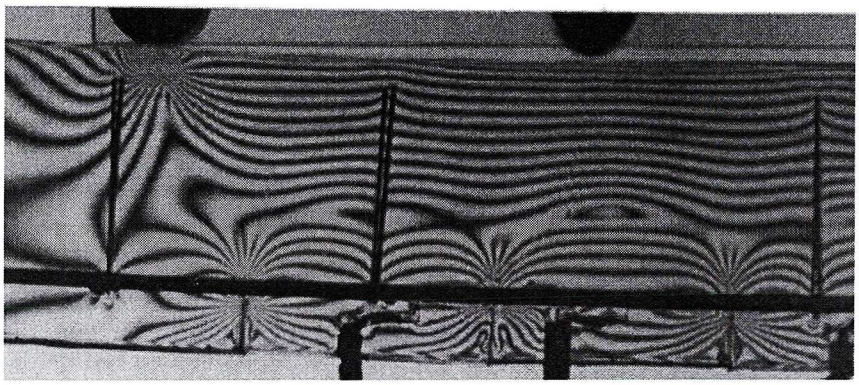

Fig. 22. Distribution of isochromatic fringes (σ_1-σ_2) obtained experimentally, corresponding to the crtical load before the propagation of the cracks

The Rice J integral obtained by FEM (equal the strain energy release rate G_C):
$J_v \equiv 0.493$ kN/m, $K_{IC} \equiv (E_m \cdot J)^{1/2} = 1.304$ MPa·m$^{1/2}$

a) Isochromatic fringes (σ_1-σ_2)

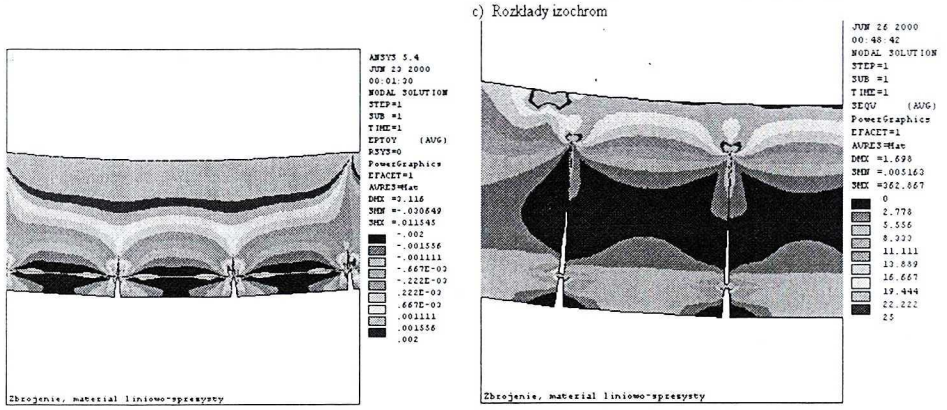

c) stresses σ_y

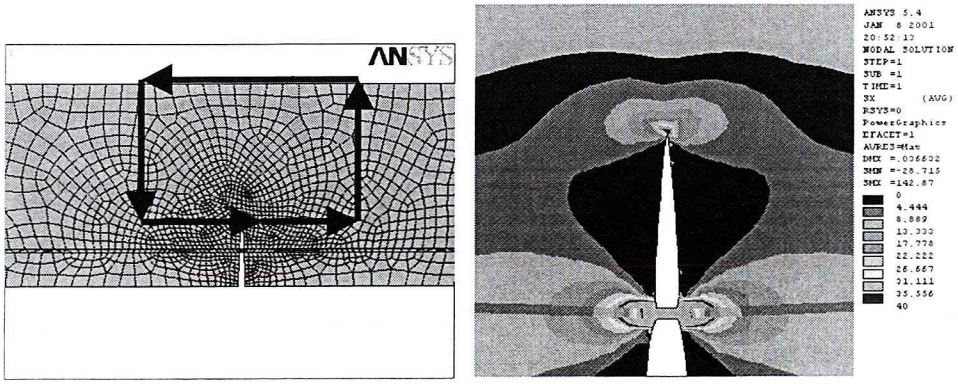

Fig. 23. Numerical simulation of cracking; a) Distribution of isochromatic fringes (σ_1-σ_2); b) the strains ε_y and the stresses σ_y, correspondings to the propagation of the crack; c) the integral path from which one calculated the value of the Rice J integral

5. 2. Fracture in direction parallel to the beam axis

The Rice J integral obtained by FEM (equal the strain energy release rate G_C):
$J_h \cong 0.699$ kN/m, $K_{IIC} \cong (E_m \cdot J)^{1/2} = 1.55$ MPa·m$^{1/2}$

a) Isochromatic fringes (σ_1-σ_2)

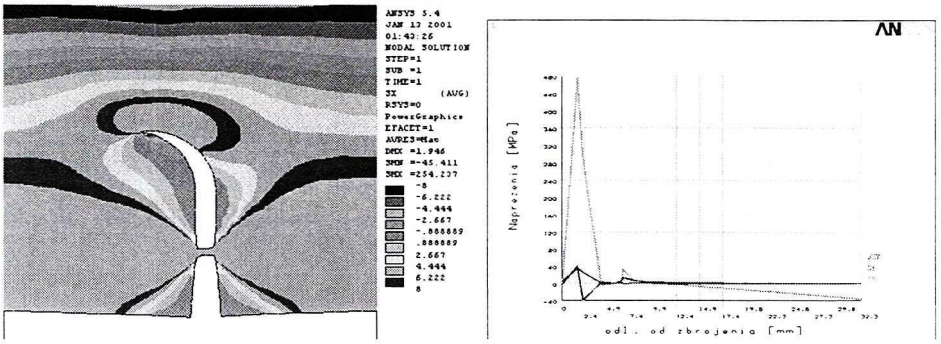

b)

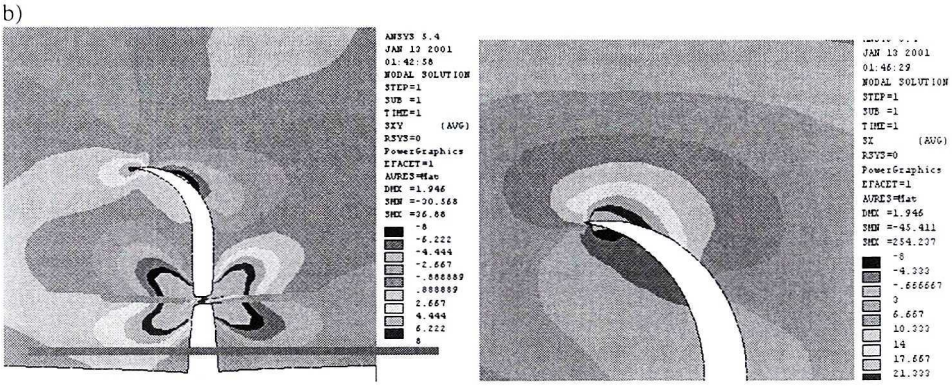

c)

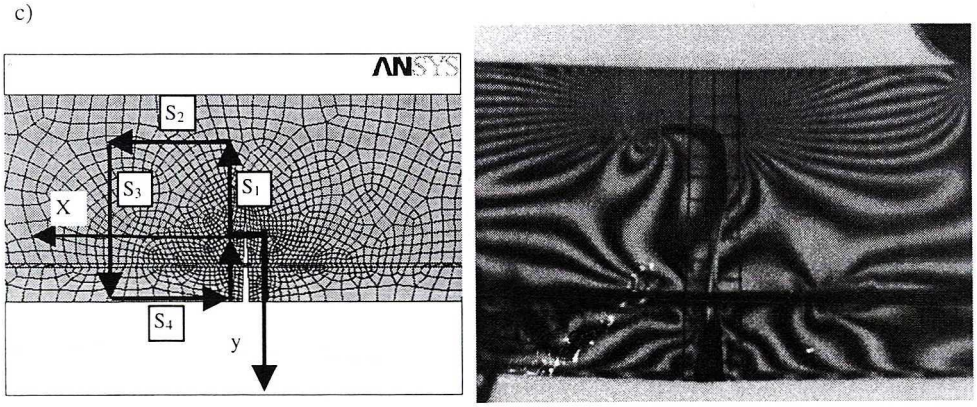

Fig. 24. Isochromatic fringes (σ_1-σ_2) and corresponding the stresses parallel to the beam axis propagation of the crack, a) distribution of the isochromatic fringes b) stresses σ_x, σ_y and τ_{xy} c) the integral path from which one calculated the value of the Rice J integral the experimental isochromatic fringes distribution are shown for comparison

6. Conclusions

In the case of composite elements made of synthetic optically active resins, there is a possibility to analyse the failure phase by means of the photoelastic method, on the basis of model, tests directly in the structure. This method makes it possible to determine the critical values of the strain energy release rate (G_C) and the stress intensity factors (K_I and K_{II}) corresponding to the mixed mode fracture based on experimental results.

The Author decided to test a series of beams: 1) Models reinforced classically by copper bars and steel. 2) Models reinforced linearly by fibber kevlar and carbon. Finite element calculations (FEM) were performed in order to verify the experimentally observed branching phenomenon and the isochromatic distribution observed during cracks propagation along debonded parts.

The theoretical ultimate bending moment was derived using the strain energy release rate (G_C) and the stress intensity factors (K_I and K_{II}) corresponding to the crack propagation of the matrix and the yield limit stress in the reinforcement.

The fracture in the reinforced composite elements subjected to bending and their strength are closely dependent on several processes: matrix cracking, fiber plastic deformation or failure, interfacial debonding between matrix and fibers. The criterion to calculate the maximum load was derived from two processes only: matrix cracking and the plastic deformation of the reinforcement.

The fracture criterion for combined loading in both mode I and mode II can by expressed in terns of the stress intensity factors (K_I and K_{II}) in the form (32) and (33). The experimental results confirmed the validity of the hypothesis that the empirical equation (32) can by considered as a practical criterion for reinforced composite elements.

Manuscript received by Editorial Board, May 25, 2001;
final version, November 29, 2001.

REFERENCES

[1] Bosco C., Carpinteri A.,Debernardi P. G.: Fracture of reinforced concrete: scale effect and snap-back instability. Engineering Fracture Mechanics, Vol. 35, No4/5, 1990. p. 665÷677.

[2] Frocht M. M.: Photoelasticity. John Wiley, New York 1960.

[3] Chisholm D. B., Jones D. L.: An analytical and experimental stress analysis of a practical mode II fracture test specimen. Experimental Mechanics 1977, 1.

[4] Irwin G.R., Dally J.W., Kobayashi T., Fourney W.L., Etheridge M.J., RossmanithH.P.: On the determination of the a-K relationship for birefringent polymers. Experimental Mechanics 1979, 19 (4).

[5] Gross B., Srawley J. E.: Stress-intensity factors for single edge noth specimen in bending or combined bending and tension by boundary collocation of a stress function. NASA Technical Note D-2603, 1965.

[6] Srawley J. E., Gross B.: Stress-Intensity Factors for bent and compact specimens. Eng. Fract. Mech. 1972, 4, pp. 587÷589.

[7] Hoyniak D., Conway J. C.: Finite element analysis of the compact shear specimen, Eng. Fract. Mech. 1979, 12, pp. 301÷306.
[8] Neimitz A.: Mechanika Pękania (Fracture Mechanics). PWN, Warszawa 1998.
[9] Cherepanov G. P.: Mechanics of brittle fracture. Mc Graw – Hill, New York 1979.
[10] Jaroniek M.: Propagation of cracks in models a reinforced concrete beam. Elsevier Science Publishers LTD, London, New York 1991.
[11] Kapkowski J., Słowikowska I., Stupnicki J.: Badanie naprężeń metodą elastooptycznej warstwy powierzchniowej. PWN, Warszawa 1987.
[12] Okamura H., Watanabe K., Takano T.: Deformation and Strength of Cracked Member Under Bending Moment and Axial Force, Eng. Fract. Mech. 1975, 7, pp. 531÷539.
[13] Sanford R. J., Dally J. W.: A General Method For Determining Mixed-Mode Stress Intensity Factors From Isochromatic Fringe Patterns. Eng. Fract. Mech. 1979, Vol. 2, p. 621÷633.
[14] Sih G. C.: Hanbook of Stress-Intensity Factors, Bethlehem, Leigh University Press, Vol. 1, 1973.
[15] Sih G. C.: Strain-energy-density factor applied to mixed mode crack problems. Int. J. of Fract. 1974, 10, pp. 305÷321.
[16] Schindler H.J., Sayir M. Path of crack in a beam due to dynamic flexural fracture. Int. J. of Fract. 1984, 25, pp. 95÷107.
[17] Szczepiński W.: A photoelastic method for determining stresses by means isochromes only. Archiwum Mechaniki Stosowanej. 5 (13) 1961.
[18] Szmelter J.: The Finite Element Method Programs, Arkady, Warsaw 1979.
[19] Sahn S., Goldner H.: Bruch – und Beurteilungkriterien in der Festigkeitslehere. VEB Fachbuchverlag Leipzig 1989.
[20] Tada H., Paris P., Irwin G. R.: The stress analysis of cracks: Handbook. – Hellertown: Del Research Corp. 1973, p. 385.
[21] Rice J. R.: A Path Independent Integral and the Approximate Analysis of Strain Concentration by Notches and Cracks. Journal of Applied Mechanics1968, p.379.
[22] Wessel E. T.: State of the art of the WOL specimen for fracture toughness testing. Eng. Fract. Mech. 1979, 12, pp. 99÷101.
[23] Williams J. G.: Fracture Mechanics of Polymers. Ellis Horwood Limited John Wiley & Sons, New York – Chichester 1984.
[24] Williams M. L.: On the Stress Distribution at the Base of a Stationary Crack. Trans. ASME, Journal of Appl. Mechanics. 1961, 12, pp. 78÷82.
[25] Wu E. M.: Application of Fracture Mechanics to Anisotropic Plates, Trans. ASME, Journal of Appl.Mechanics. E, 1967, 34, pp. 967÷974.
[26] Zienkiewicz O. C.: The Finite Element Method in Engineering Science. Mc Graw – Hill, London, New York 1971.

Eksperymentalna i numeryczna analiza zbrojonych elementów kompozytowych poddanych zginaniu

Streszczenie

Kruche pękanie elementów kompozytowych jest istotnym problemem analizowanym przez konstruktorów od wielu lat i analiza sposobu zniszczenia zajmuje centralną pozycję przy

rozwiązywaniu tego problemu. W pracy przedstawiono przykłady i porównano wyniki badań eksperymentalnych i obliczeń numerycznych elastooptycznych modeli belek zbrojonych.

Procesy pękania elementów kompozytowych zbrojonych prętami, lub pasmami są dosyć złożone, zniszczenie może być spowodowane pękaniem matrycy, utratą nośności zbrojenia, delaminacją zbrojenia, lub inaczej mówiąc utratą przyczepności zbrojenia i matrycy (spowodowaną tzw. pękaniem międzyfazowym).

W pracy niniejszej przedstawiono kolejne fazy zniszczenia belek kompozytowych z żywic syntetycznych zbrojonych prętami, lub pasmami w strefie rozciąganej, narażonej na pękanie oraz określono wielkość współczynnika uwalniania energii sprężystej w złożonym sposobie zniszczenia elementu. Przedstawiono także uproszczoną metodę określania nośności belek zbrojonych na podstawie parametrów mechaniki pękania matrycy K_{IC}, K_{IIC} i G_C oraz nośności zbrojenia. Wprowadzając do obliczeń założenia mechaniki pękania, można wyznaczyć graniczne wartości obciążeń w funkcji współczynników intensywności naprężenia K_I, K_{II} i współczynnika uwalniania energii sprężystej (G_C) oraz odkształceń zbrojenia (sprężystych lub plastycznych). Zastosowana metoda umożliwia jakościową ocenę propagacji pęknięć w poszczególnych fazach zniszczenia elementu.